nature energy

REVIEW ARTICLE

https://doi.org/10.1038/s41560-018-0190-4

Opportunities and challenges for tandem solar cells using metal halide perovskite semiconductors

Tomas Leijtens[1,2*], Kevin A. Bush[1], Rohit Prasanna[1] and Michael D. McGehee[1*]

Metal halide perovskite semiconductors possess excellent optoelectronic properties, allowing them to reach high solar cell performances. They have tunable bandgaps and can be rapidly and cheaply deposited from low-cost precursors, making them ideal candidate materials for tandem solar cells, either by using perovskites as the wide-bandgap top cell paired with low-bandgap silicon or copper indium diselenide bottom cells or by using both wide- and small-bandgap perovskite semiconductors to make all-perovskite tandem solar cells. This Review highlights the unique potential of perovskite tandem solar cells to reach solar-to-electricity conversion efficiencies far above those of single-junction solar cells at low costs. We discuss the recent developments in perovskite-based tandem fabrication, and detail directions for future research to take this technology beyond the proof-of-concept stage.

Rapid cost reductions in photovoltaic module manufacturing have made non-module costs (known as balance-of-system costs) and installation costs the major contributors to the price of installed solar in both residential and utility settings[1]. These costs scale with the solar panel area required, making the efficiency of photovoltaic panels one of the most important and promising technical directions for reducing the cost of solar installations. The efficiencies of crystalline-silicon (c-Si) and thin-film technologies, such as CdTe and copper indium gallium selenide (CIGS), have started to saturate at ~26% and 23%[2], respectively, and are limited to the fundamental Shockley–Queisser (SQ) limit of 31–33 % for single-junction (SJ) solar cells. Multi-junction solar cells, comprising multiple absorber layers with complementary bandgaps, offer a proven approach to reach significantly higher performances. III–V compound semiconductors, sometimes in conjunction with Ge, have been employed to make efficient (39% under 1 sun) multi-junction solar cells with up to five different absorber layers[2–4]. Unfortunately, these materials require complicated and costly manufacturing processes and substrates. Other than III–V compounds, established semiconductor systems do not offer a wide range of bandgaps capable of high performances[5,6], leaving no cost-effective solution for high-efficiency tandem solar cells.

Solar cells comprising polycrystalline films of metal halide perovskite semiconductors have recently attracted attention for their potential to be processed at low cost from commonly available precursors[7–9] via both solution[10] and vapour deposition routes[11]. Crucially for tandem applications, their bandgaps can be tuned by simple substitution of chemical elements on the A, B and X sites of the ABX_3 crystal structure, yielding functioning solar cells with a range of bandgaps between 1.18 and 2.3 eV (refs [12–15]). As a result, perovskite solar cells are attractive candidates for use in tandem solar cells, both in hybrid configurations where they are paired with more established bottom cells such as c-Si and CIGS or in all-perovskite tandem solar cells.

This Review will explore the potential for perovskite-based tandem cells. We will discuss the unique promise of metal halide perovskites for multi-junction solar cell applications, highlight current developments of perovskite tandems and discuss the work that remains to be done to bridge the gap to commercial readiness. As laboratory-scale devices continue to exhibit high efficiencies, proving the potential of perovskite tandem solar cells, it will become increasingly important to consider the design of the tandem devices holistically to ensure that they are translatable to commercial manufacturing and operation in real-world conditions.

Tandem solar cells and the promise of perovskites

Multi-junction (tandem) solar cells mitigate losses that come from carrier thermalization by using several semiconductor layers with different bandgaps. In a double-junction tandem, a 'top cell' with a large bandgap absorbs high-energy photons but permits lower-energy photons to pass through to be absorbed in the 'bottom cell', which has a small bandgap. In this way, the higher-energy photons generate a high voltage in the top cell while the low-energy photons are absorbed in the bottom cell, raising the obtainable efficiency of the combined tandem cell over that of either a single high- or low-bandgap solar cell.

Figure 1 depicts plots of theoretical double-junction tandem solar cell power conversion efficiencies (PCEs) versus bottom and top cell bandgaps in both monolithic two-terminal (2T) (Fig. 1a) and mechanically stacked four-terminal (4T) configurations (Fig. 1b) along with the bandgap combinations used in current state-of-the-art perovskite-based tandems as reported in the literature (performance parameters given in Table 1). 2T tandems consist of two series-connected subcells of different bandgaps, so that the current through each subcell must be identical, resulting in a 'current matching' requirement. Because 4T tandems are not necessarily connected in series, they are not limited by current matching, making them less sensitive to the exact bandgap combination chosen. They are easier to prototype, but suffer from parasitic absorption and reflections from additional transparent reflections and interfaces, which should ultimately result in lower practical efficiencies. The figure demonstrates that it is critical to select absorbers with

[1]Materials Science and Engineering, Stanford University, Stanford, CA, USA. [2]Present address: Materials Science Center, National Renewable Energy Laboratory, Golden, CO, USA. *e-mail: Tomas.Leijtens@nrel.gov; mmcgehee@stanford.edu

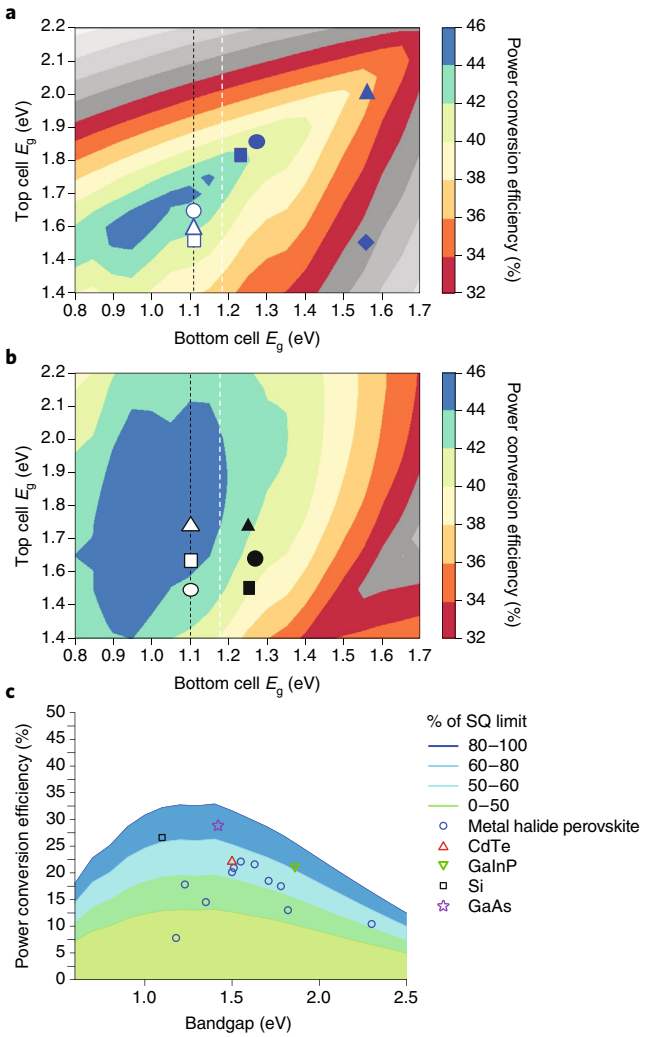

Fig. 1 | Comparison of theoretical tandem performance limits and current best devices. a, Theoretical efficiency limit for 2T tandems, calculated with different subcell thicknesses, each picked to optimize the performance for each bandgap combination. Grey shading signifies anything below the SQ limit of 32% for a SJ with a 1.1 eV bandgap, indicating where there is no efficiency gain in building a tandem device. The dotted white lines mark the lowest bandgap currently accessible to metal halide perovskite semiconductors. The solid symbols indicate bandgap combinations thus far used in making all-perovskite tandems (details in Table 1). The black dashed line marks the 1.12 eV bandgap of silicon, while the open symbols represent the bandgap combinations for the best-achieved 2T perovskite–Silicon tandems. **b**, The same plot is provided for 4T tandems. The theoretical efficiency was calculated as follows. The short-circuit current was calculated by integrating the AM1.5G spectrum assuming 100% EQE above the bandgap. The reverse saturation current was calculated from detailed balance as by Shockley Queisser in 1961[102] assuming 100% radiative emission. From these quantities, an *I*–*V* curve was simulated assuming the ideal diode equation applies. For a monolithic (series-connected) tandem, the short-circuit current was taken to be the current in the wide-gap cell or half the current produced by the low-gap cell (whichever is smaller), and then Kirchhoff's rule applied to combine the *I*–*V* curves of the two subcells and determine a tandem efficiency. For mechanically stacked tandems, these constraints do not apply, and the efficiency was simply taken as the sum of the efficiencies of the best possible subcells. **c**, SJ record power conversion efficiencies, plotted as a function of perovskite bandgap and compared to the SQ limit (references in Supplementary Table 1). Different fractions of the detailed balance limit are denoted by the different colour shadings on the plot.

appropriate bandgaps for both subcells, especially when developing 2T tandems, and that bandgap combinations with high efficiency limits are readily accessible for metal halide perovskite absorbers. As demonstrated in Fig. 1c, metal halide perovskite semiconductors can be designed to meet these requirements; solar cells have already been made with bandgaps from 1.18–2.3 eV, while >17% solar cells have been developed within the slightly narrower window of bandgaps of 1.25–1.8 eV, enabling limiting tandem efficiencies of ~42%. Currently, perovskite–perovskite tandems have reached 18.5%[16] and 22.9%[17] in 2T and 4T configurations, with the 4T surpassing the single-junction record already.

The black dotted line in Fig. 1a,b represents the ~1.1 eV bandgap of c-Si and the best performing CIGS solar cells. These could be ideally paired with perovskites in the 1.6–1.75 eV range to yield limiting performances of ~44%. This type of 'hybrid' tandem approach, where perovskites provide a boost in efficiency for little additional cost, presents an exciting path to delivering higher-efficiency panels without significant additional costs or changes to existing c-Si manufacturing lines and supply chains. This may be the most direct pathway to commercializing perovskite-based photovoltaics, and also one of the fastest routes to realizing a step improvement in commercially available c-Si module efficiencies. As a result, the perovskite–Si tandem has been the focus of a great deal of research and has recently reached efficiencies of 23.6%[18] and 26.4%[19] in 2T and 4T configurations, respectively, approaching the world record c-Si performance of 26.6%[20]. In both cases, the tandem solar cell has >25% greater efficiency (relative) than the SJ silicon solar cell used as the bottom cell. We view the perovskite–Si tandem as the first step towards commercialization of perovskite tandem devices, while the all-perovskite tandem may be the ultimate goal, presenting an exciting opportunity for high-efficiency modules with all the advantages inherent to thin-film photovoltaics (PV) manufacturing: high throughput, low cost and the ability to use flexible and light substrates.

Figure 1c depicts the SJ SQ limit as a function of bandgap and demonstrates that almost the entire range of available perovskite bandgaps can attain over 50% (but less than 80%) of the SQ limit, letting them rival materials such as c-Si, CdTe and GaInP (refs [2,21]). These high performances over a wide range of bandgaps, together with the ability to be manufactured at low cost, make perovskite–perovskite and perovskite–silicon tandems extremely attractive. Box 1 discusses progress made in cost modelling of perovskite solar cells and takes learnings from single-junction devices to tandem solar cells to demonstrate that tandem solar cells should benefit from very low additional costs over those of single-junction solar cells, but provide the advantage of substantially superior performances. For this to translate to a low levelized cost of electricity, not only does the device lifetime need to be long, but the energy yield of the tandem solar cells must be high over the course of many seasons and varying solar irradiation spectra. Though the current-matching requirement across subcells in 2T configurations could be expected to result in drastic drops in performance as the solar spectrum varies, recent work has demonstrated, as is discussed in detail in Box 2, that the efficiency advantage of tandem solar cells under AM1.5 conditions is not affected by the variations in solar spectrum across an entire year, even in locations with high cloud cover such as Seattle.

Wide-bandgap perovskite absorbers for top cells

A tandem solar cell surpasses the performance of single-junction solar cells by minimizing thermalization losses of high-energy photons, so it is imperative that efficient wide-bandgap cells are used to maximize tandem voltage and performance. Top and bottom cell partners should be chosen based on each cell's spectral efficiency[22]. Spectral efficiency is the fraction of a photon's energy of a given wavelength that is converted to electrical energy, so a top cell will

Table 1 | Tandem efficiencies

	Si or perovskite bottom cell	Perovskite top Cell	PCE (%)	J_{sc} (mA cm^{-2})	V_{oc} (V)	FF	Symbol for Fig. 1	Ref.
4T	IBC c-Si	$FA_{0.75}MA_{0.15}Cs_{0.10}Rb(I_{0.66}Br_{0.33})_3$ + 5% RbI (1.63 eV)	26.4	19.4, 18.8	1.12, 0.73	0.73, 0.80	□	19
4T	SHJ c-Si	$MAPbI_3$ (1.55 eV)	25.2	20.1, 16.0	1.07, 0.69	0.76, 0.80	○	91
4T	SHJ c-Si	$FA_{0.83}Cs_{0.17}Pb(I_{0.6}Br_{0.4})_3$ (1.74 eV)	19.8	19.9, 13.9	1.10, 0.69	0.71, 0.76	△	81
4T	TI mc-Si	$MAPbI_3$ (1.55 eV)	17.0	17.5, 11.1	1.03, 0.55	0.71, 0.70	○	92
2T	SHJ c-Si	$FA_{0.83}Cs_{0.17}Pb(I_{0.83}Br_{0.17})_3$ (1.63 eV)	23.6	18.1	1.65	0.79	○	18
2T	n-type HJ c-Si	$Cs_{0.07}Rb_{0.03}FA_{0.765}MA_{0.135}Pb(I_{0.85}Br_{0.15})_3$ (1.62eV)	22.5	17.6	1.75	0.73	○	45
2T	SHJ c-Si	$Cs_{0.19}MA_{0.81}PbI_3$ (1.58 eV)	22.0	16.8	1.75	77.5	△	44
2T	SHJ c-Si	$MAPbI_3$ (1.55 eV)	21.2	15.9	1.69	0.80	□	41
2T	SHJ c-Si	$MAPbI_3$ (1.55 eV)	18.1	14.0	1.76	0.77	□	42
2T	n-type, HJ	$MAPbI_3$ (1.55 eV)	13.7	11.5	1.58	0.75	□	59
4T	$FA_{0.6}MA_{0.4}Sn_{0.60}Pb_{0.40}I_3$ (1.25 eV)	$FA_{0.8}Cs_{0.2}Pb(I_{0.7}Br_{0.3})_3$ (1.75 eV)	22.9	17.5, 12.3	1.20, 0.81	0.74, 0.74	▲	93
4T	$FA_{0.6}MA_{0.4}Sn_{0.60}Pb_{0.40}I_3$ (1.25 eV)	$MAPbI_3$ (1.55 eV)	21.0	20.1, 4.8	1.14, 0.81	0.80, 0.74	■	17
4T	$FA_{0.75}Cs_{0.25}Sn_{0.50}Pb_{0.50}I_3$ (1.27 eV)	$FA_{0.83}Cs_{0.17}Pb(I_{0.83}Br_{0.17})_3$ (1.63 eV)	20.3	20.3, 7.9	0.97, 0.74	0.79, 0.73	●	12
2T	$MASn_{0.50}Pb_{0.50}I_3$ (1.22 eV)	$MA_{0.9}Cs_{0.1}Pb(I_{0.6}Br_{0.4})_3$ (1.82)	18.5	12.3	1.98	0.73	■	16
2T	$FA_{0.75}Cs_{0.25}Sn_{0.50}Pb_{0.50}I_3$ (1.27 eV)	$FA_{0.83}Cs_{0.17}Pb(I_{0.50}Br_{0.50})_3$ (1.85 eV)	17.0	14.5	1.66	0.70	●	12
2T	$MAPbI_3$ (1.55 eV)	$Fa_{0.85}Cs_{0.15}Pb(I_{0.30}Br_{0.70})_3$ (2 eV)	18.1	9.8	2.29	0.80	▲	58
2T	$MAPbI_3$ (1.55 eV)	$MAPbI_3$ (1.55 eV)	7.0	6.6	1.89	0.56	◆	57

IBC, interdigitated back contact solar cells; SHJ, silicon heterojunction solar cells; HJ, homo-junction solar cells; TI, low grade multicrystalline silicon solar cells. The PCEs are extracted from the steady state measurements where provided, while the J_{sc}, V_{OC} and fill factor (FF) are from the scanned current–voltage characteristics. The two values presented in each of the J_{sc}, V_{OC} and FF columns represent the values for the front cell and the rear cell of the tandem solar cell, respectively. The symbols can be used to find the particular bandgap combination in Fig. 1a,b.

only improve the efficiency of a bottom cell if it has a higher efficiency resolved at a given wavelength. Figure 2a shows the spectral efficiencies of the most promising perovskite top cell candidates and the best perovskite and c-Si bottom cells and demonstrates that the spectral efficiencies at low wavelengths for the wide-bandgap (1.55–2.3 eV) perovskite solar cells are considerably higher than those for c-Si and small-bandgap perovskite bottom cells. Because the external quantum efficiencies (EQEs) of most perovskite solar cells are very high, the main limiting factor to spectral efficiency of top cells is the fill factor (FF) and the open-circuit voltage V_{OC}, which can also be expressed as a loss in potential.

Some perovskite compositions already display losses in potential comparable to the best semiconductors such as GaAs and silicon (0.37 V loss[23]): 0.33 V for a 1.25 eV bandgap[24], 0.36 V for a 1.57 eV bandgap[25], and 0.39 V with a 1.63 eV bandgap. Ideally, these low voltage losses would be universal to halide perovskites of any composition. However, voltage has thus far not tracked linearly with increasing bandgap in bromide-rich perovskite compounds and the loss in potential increases with bandgap, see Fig. 2b. This leads to the striking observation that the 1.75 eV cells[26] do not surpass the spectral efficiency achieved by the 1.63 eV quadruple cation cells[27] or 1.55 eV record perovskite solar cells[28] (Fig. 2a). According to these two plots, high-efficiency compositions in the 1.55–1.63 eV range display the most promising characteristics (among existing compositions) for top cells in tandems both because they have higher spectral efficiencies and because they will be more stable under operation due to lower Br contents[18,27]. Indeed, a top cell bandgap of 1.63 eV can still achieve a limiting efficiency of 43% on c-Si bottom cells and 39% on perovskite bottom cells (Fig. 1a)[29]. A coupled optical and device model has been used[30] to determine ideal bandgap combinations for all-perovskite tandems, and demonstrates that the present generation of 1.63 eV top cells in a perovskite–silicon tandem can still yield a practical tandem performance over 31% and 29.5%[30] in an all-perovskite tandem.

Further improvements would be obtained by minimizing the loss in potential of wider-bandgap perovskites. There may be several reasons for the fact that the V_{OC} and hence spectral efficiency do not follow bandgap in perovskite solar cells. The most studied is that on illumination, halide segregation into I-rich and Br-rich regions (a process termed the Hoke effect)[31] occurs and limits the Fermi level splitting to that of the lower-bandgap I-rich regions, which effectively act as trap sites. Two thorough reviews respectively highlight the current understanding[32] and demonstrate[15] that while compositional tuning of the A and X site in three-dimensional (3D) perovskite structures and surface passivation[33] offer some promise, no definite solution has been found for obtaining photostable 3D perovskite compositions approaching the 1.8 eV bandgaps most desirable for all-perovskite tandems. In addition, carrier lifetimes for bromide-containing high-bandgap materials have remained lower than those of the more heavily studied iodide materials, even when the Hoke effect does not occur. It is unclear whether the fast non-radiative recombination is due to unique bromide-related defects, wider bandgaps exposing trap levels hidden within the bands for smaller bandgap materials, or simply the result of the bromide-containing wide-bandgap materials and associated selective contacts being less studied and optimized.

Narrow-bandgap perovskites for all-perovskite tandems

All-perovskite tandems offer a route to high efficiency while maintaining the benefits of low-cost and low-temperature fabrication

Box 1 | Costs

Published technoeconomic analyses[94–96] lead to ranges in expected perovskite SJ module costs of ~US$30–120 m^{-2}, and all three studies agree that the materials costs generally dominate the module cost (>90% of total costs). Replacing impractical materials (for example, gold, custom synthesized organic molecules[95]) from the perovskite solar cell stack with lower cost materials such as SnO_2, NiO_x and commonly used electrode materials such as ITO, IZO and Al yields a module cost structure (~US$30 m^{-2}) that is only weakly dependent on the perovskite and contact layer costs (~US$2 m^{-2} combined)[94,96]. We can learn from these SJ models for tandem solar cells: the substrate and back cover (both glass) are the limiting factor in cost of any perovskite solar cell of this type, contributing ~US$10 m^{-2}, followed by the junction box (~US$7 m^{-2}), module lamination and packaging (~US$6 m^{-2}) and transparent conductive oxide deposition (~US$3 m^{-2}). These numbers agree with cost predictions for CIGS modules[97,98] and do not vary significantly within a large range of manufacturing throughput.

Since 2T tandems do not require additional substrates, packaging or junction boxes, the additional costs relative to SJ perovskite or silicon solar cells should be dictated by the top cell perovskite active layer, selective contacts and the TCO. These are estimated to be no more than ~US$10 m^{-2}, compared to the already present costs of ~US$70–80 m^{-2} for a commercial c-Si module as the bottom cell. Tandem solar cells may need additional protective layers (such as SnO_2) to enable sputter coating of transparent electrodes, but currently used ALD and CVD routes[18] can be cost effective at scale depending on precursors used[99].

The analysis above implies that the tandems should provide a >~15% relative boost in efficiency to be able to lower the cost per watt peak (W_P) of the modules. There is added value to a higher-efficiency module as a 4% absolute increase in module efficiency can reduce the area-related balance-of-systems costs by ~US$0.03 per W_P and US$0.06 per W_P for utility scale and rooftop solar installations, respectively[100]. Taking these preliminary costing studies together with the realistically obtainable cell level efficiencies near 30% high annual energy yield[29], the perovskite–Si tandems seem poised to be a success provided that the perovskite top cell does not limit the tandem stability.

All-perovskite tandems offer the promise of even lower manufacturing costs associated with roll-to-roll thin-film manufacturing, as well as the allure of efficient but lightweight and flexible photovoltaic modules. Assuming a similar cost structure to those published for SJ perovskite solar cells, but incorporating additional contact layers, a small-bandgap perovskite layer and an extra TCO (for the recombination layer), costs below ~US$40 m^{-2} should be achievable for a device architecture capable of nearing 30% power conversion efficiency at the cell level and > 25% at module level, translating ultimately to <US$0.16 per W_P. Unfortunately, cost-effective flexible encapsulation is still under development, raising costs of flexible all-perovskite tandems over those of rigid, glass packaged modules.

as well as the possibility of lightweight, flexible form factors for both subcells in the stack. So far, all perovskites[14,16,17,34–37] useful as bottom cells in tandems require both tin and lead on the B-site to achieve low bandgaps. The best-performing single-junction cell with a narrow-gap perovskite reported so far uses $FA_{0.6}MA_{0.4}Sn_{0.6}Pb_{0.4}I_3$ (where MA is methylammonium and FA is formamidinium), achieving 17.8% PCE with a bandgap of 1.25 eV (refs [17,37]) and yielding a (21%) 4T tandem[17]. Perovskites with still smaller bandgaps ($MASn_{0.8}Pb_{0.2}I_3$ with 1.19 eV (ref. [38])) have been reported, but have not yet yielded solar cells with >10% PCE. Using perovskites with smaller bandgaps is desirable to get closer to the ideal bottom cell bandgap for a 2T tandem (Fig. 1a), and because it enables the use of more stable, smaller-bandgap perovskites for a current-matched top cell as described above.

Properties and challenges facing Sn–Pb perovskites. Tin–lead perovskites have lower absorption cross-sections than pure lead perovskites, though it isn't yet clear why. This implies that monolithic perovskite tandems and single-junction low-bandgap perovskite solar cells have been limited by low short-circuit currents due to low external quantum efficiency in the near-infrared (NIR)[12,16]. To obtain an EQE of higher than 80% across the spectrum, which will be essential for optimal current matching in a tandem, it has been necessary to use tin–lead perovskite layers that are over 1 μm thick for the bottom cell[17]. This in turn requires carrier diffusion lengths to be at least 3 μm to allow efficient extraction of photogenerated charge. Early reports of tin perovskites showed extremely short carrier lifetimes of well below a nanosecond[12,39], but lifetimes of hundreds of nanoseconds have been achieved by compositional tuning on the A-site using methylammonium (MA) and formamidinium (FA) and optimizing processing conditions with antisolvent techniques to produce large grains[16,17]. These developments should lead to improved tandem solar cell performances once implemented into tandem designs.

On the other hand, many Sn–Pb perovskites display high open-circuit voltages relative to their bandgap[38]. The loss-in-potential ($E_g - qV_{oc}$), where E_g denotes the energy of the bandgap in electron volts and q is the elemental charge, reported for these perovskites is as low as 0.33 eV (ref. [24]) (Fig. 1d), which is the smallest reported for any perovskite solar cell[27] and is even better than the loss-in-potential of the best crystalline silicon solar cells[20]. Recent optical and device modelling shows that all-perovskite tandems based on the best-reported small- and wide-bandgap perovskite solar cells can exceed 30% in performance with EQEs over 90% and high V_{OC} when thick (700–1,000 nm) absorber layers are used[30], making this technology potentially very competitive performance-wise with perovskite–silicon tandems provided that stability concerns over Sn-based perovskites can be overcome[39,40].

Fabrication challenges in perovskite tandem solar cells

To help clarify the processing of tandem solar cells and to give context for each of the subsections below, basic process flows are provided for perovskite–Si and all-perovskite tandem solar cells in Fig. 3. The tandem device architectures and layers used within them that are described in the sections below are depicted in Fig. 4.

Transparent conducting electrode. Unlike in a single-junction perovskite solar cell, the top transparent electrode (usually a transparent conducting oxide, TCO) in many tandem architectures (both 2T and 4T) must be deposited on top of the perovskite cell to allow light to enter into the device. To prevent sputter damage to the soft layers comprising perovskite solar cells, research groups have had to develop protective 'sputter buffer' or 'sputter barrier' layers[12,18,41,42]. These are typically thin (5–30 nm) so as not to negatively impact electronic transport properties, and this has spurred a shift from solution-processed layers[43] to conformally deposited vapour phase layers to enable deposition on even rough perovskite surfaces[12,18,41,42]. These deposition processes must be at a low enough temperature

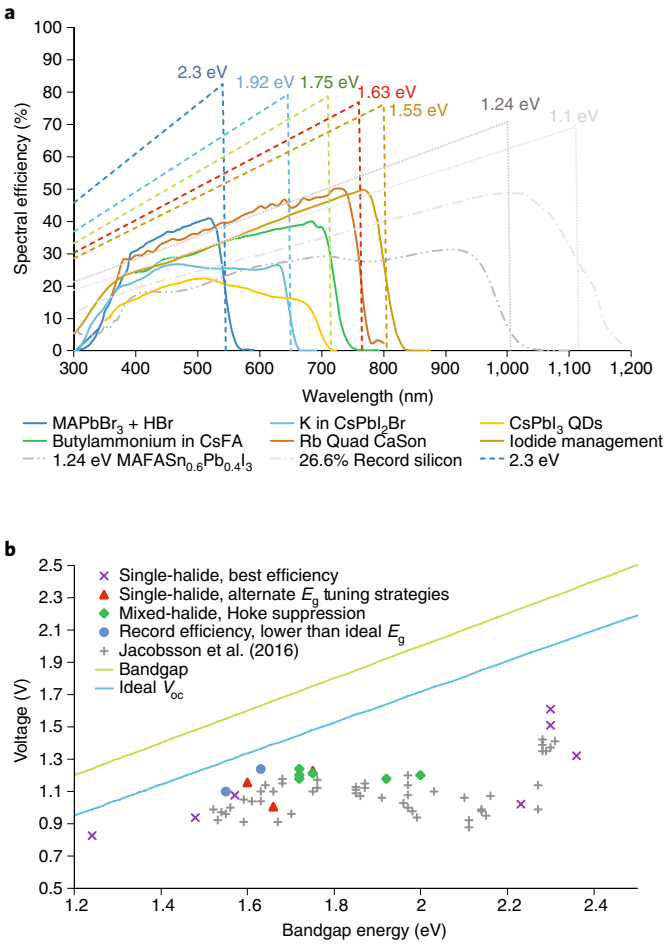

Fig. 2 | Losses in wide-bandgap perovskite solar cells. a, Spectral efficiency of various potential perovskite top cell candidates, calculated using a published model[22] (solid lines). The curves were plotted using EQEs, FF and V_{OC} from $MAPbBr_3$ solar cells[103] (dark blue), $CsPbI_3$ with potassium incorporation to stabilize the black phase[104] (light blue), $FA_{0.83}Cs_{0.17}Pb(I_{0.60}Br_{0.40})_2$ with butylammonium incorporation to make a 2D/3D structure[26] (green), rubidium containing 'quadruple cation' perovskite[27] (brown), and the current world record perovskite solar cell[60] (light brown). The theoretical (coloured dashed lines) spectral efficiency according to detailed balance is provided for several relevant bandgaps for reference. The spectral efficiencies of the current best low-bandgap perovskite[37] (dark grey) and c-Si (ref. [20]) (light grey) cells are also provided. Spectral efficiency = $q \times V_{OC} \times FF \times EQE$ at a given wavelength divided by energy of photons at that wavelength. **b**, The open-circuit voltage of SJ perovskite solar cells of varying bandgaps is displayed and compared to the 'ideal' open-circuit voltage as determined from detailed balance. Detailed information and references for these points are provided in Supplementary Table 2.

(<100 °C) and use mild enough precursors (perovskites are sensitive to oxidation and reaction with bases) that they do not damage the underlying layers. Additionally, they should be transparent and have appropriate energy levels. Using evaporated MoO_x as a buffer on top of commonly used hole transport materials (HTMs) such as Spiro-OMeTAD (Fig. 4a,c,d) is a common approach[41,42,44,45], and was used to develop a 26.4% 4T perovskite–Si tandem[19]. Other suitable protective materials could be NiO_x and VO_x. Tandem architectures with p–i–n polarity (such as those made on commercial p-type c-Si wafers) require protective electron conducting layers. Our group first used spin-coated aluminum-doped zinc oxide (AZO) nanoparticles[43] with success and then developed an atomic layer deposited

Box 2 | Energy yield

While tandems undoubtedly offer the highest performances under AM1.5 irradiation, real-world conditions are often different and vary over the course of a year. A recent study[29] combined optical modelling with device modelling, using experimentally derived parameters, to determine that both perovskite–Si and perovskite–perovskite 2T tandems present real promise to exceed 30% and approach 34% under AM1.5 conditions. Importantly, two studies[29,101] also demonstrated that the energy yield for 2T and 4T tandems can both be expected to achieve the efficiency enhancement of the devices designed for standard testing conditions in the real world as well, and that neither thermal or optical mismatch presents any considerable additional losses in a series connected tandem. This suggests that there is no clear advantage in voltage versus current matching in 4T architectures. Additionally, the higher practical efficiency, fewer processing steps and simpler module design lets us argue that monolithically integrated 2T tandems offer greater promise than the mechanically stacked 4T tandem designs. These results would bode very well for perovskite tandems lowering the levelized cost of electricity of PV systems. On the other hand, it was found in ref. [43] that tandems (2T and 4T) offer little benefit over SJs in terms of energy yield, but made different assumptions in their modelling, basing it on a device with a high ideality factor and relatively low shunt resistance for the perovskite top cell, whereas in ref. [41] a device with low ideality factor and high shunt resistance was chosen. This results in a big difference in behaviour at low light intensities, where the top cell in ref. [43] suffers much more in V_{oc} and FF and hence limits tandem performance under low light conditions. Hence, differences in total energy yield were primarily dictated by the predicted efficiencies at low light intensities rather than in the mismatched photocurrent generation in the different subcells due to variations in irradiation spectrum throughout the course of a year. This analysis highlights the important point that the energy yield of perovskite tandems will depend heavily on the quality of the perovskite sub cells in question—high shunt resistances and ideality factors approaching 1 will be critical to enable high performances at low light intensities and resultant high energy yields.

(ALD) SnO_2 layer to yield 23.6% 2T tandems with promising stability[18] (Fig. 4b). Alternative materials could be ZnO (though prone to reacting with perovskite semiconductors) and TiO_2 (ultraviolet sensitive). The recent record all-perovskite tandems[16] do not use any special sputter buffer layer; position of the sample in relation to the plasma, gas flow, accelerating voltage and temperature in the sputter tool may all be important parameters that enabled this result.

ALD SnO_2 and sputtered TCOs also improve the stability of perovskite solar cells by preventing the release of organic cations and the diffusion and subsequent reaction of metal and iodide[18,43,46,47]. Given the volatile nature of the organic cations used on the A site in perovskite semiconductors, the low activation energy for halide vacancy formation and migration, and the propensity for metals to react with perovskite layers, it is essential to continue developing sputter buffer layers and TCOs with improved barrier properties[48–50].

Perovskite layer. Tandem processing requires perovskites that are thermally and chemically robust. ALD and chemical vapour deposition (CVD) processes often involve temperatures around 100 °C or higher for the precursors to react. The precursors themselves also tend to contain ligands and counter-reagents, such as water, ozone or hydrogen peroxide, that can degrade the perovskite[51]. In

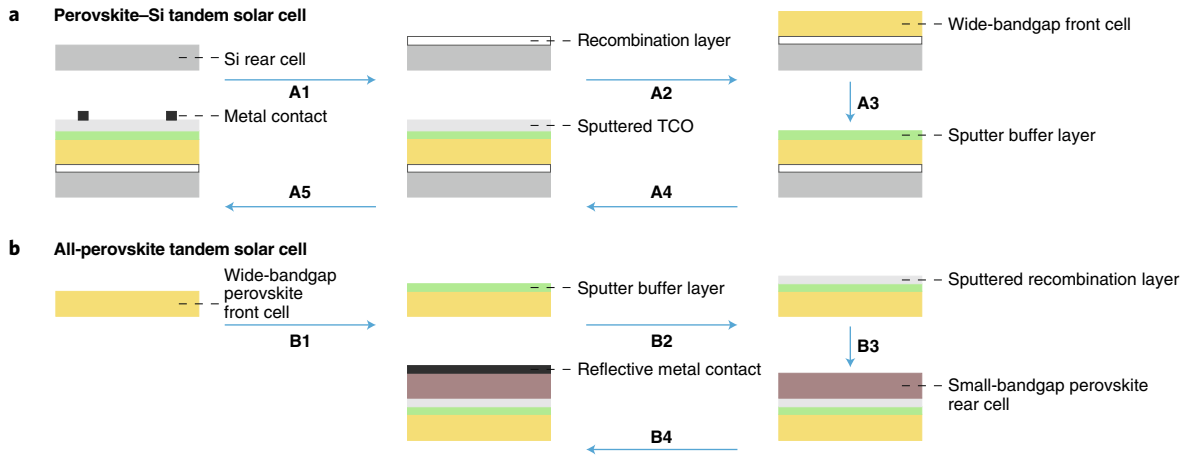

Fig. 3 | Typical tandem process flow. a,**b**, The series of steps for deposition of the most important layers in a perovskite–Si tandem solar cell (**a**) and for an all-perovskite tandem solar cell (**b**). The basic requirements for each step are explained here. For a perovskite–silicon tandem, the first step (A1) is to deposit a transparent recombination layer on the passivated front side (no reflector or solid metal electrode) of the c-Si cell. The perovskite front cell is deposited (A2) on the recombination layer using processing that does not damage the underlying recombination layer and c-Si cell. The limitations vary for different types of c-Si cell as discussed in the main text. A sputter buffer layer is deposited (A3) on the perovskite front cell to protect it from sputter damage during sputtered deposition (A4) of the front transparent electrode. The buffer layer must be transparent and conductive to the relevant electronic carrier (electrons in the case of c-Si cells made on p-type wafers and holes for tandems made on n-type c-Si wafers). The top transparent electrode must have low sheet resistance and high transparency. Finally, metal gridlines (A5) are used to minimize series resistance through the transparent conductor. For all-perovskite tandem solar cells, a wide-bandgap front cell is deposited on a transparent conducting substrate and this front cell is protected from sputter damage by depositing a sputter buffer layer (B1). A conductive, transparent recombination layer is sputtered on top of the buffer layer (B2). This recombination layer can also protect the underlying front cell from damage during solution processing of the small bandgap rear cell, which can then be deposited from solution (B3). Finally, a reflective metal electrode is used to contact the small bandgap rear cell and lengthen the light pathlength (B4). There are other possible sequences of steps and processes, but these are those taken for the majority of perovskite–Si and all-perovskite tandem solar cells.

addition, common manufacturing processes used in silicon PV lines such as gridline printing and module lamination between glass sheets with adhesive polymers, such as ethylene-vinyl acetate (EVA), often require annealing temperatures of up to 150 °C. For these reasons, the volatile MA cation[48,52] may be somewhat less suitable than FA and Cs on the A site, though further work needs to be done to understand the stability of mixed A-site cation materials[27,53].

Recombination layer. A 2T tandem requires a recombination layer to allow current to flow across the two subcells by allowing opposite carriers from the subcells to recombine in a highly doped layer. In traditional III–V multi-junction solar cells, tunnel junctions must be lattice matched to the subcells[54,55], limiting the available options. This restriction does not apply to perovskite tandems, enabling novel recombination layer designs.

Solution processed tandems made from organic molecules employ thin layers of highly doped organic (such as PEDOT:PSS) or inorganic layers (such as ZnO) as recombination layers, and this approach was adapted for perovskite–perovskite tandems with some success[56,57]. Thermally evaporated layers of doped n- and p-type organic molecules can be used as an effective recombination layer in evaporated 2T tandems[58]. A simple approach is to use a conductive transparent conducting oxide (TCO) such as indium tin oxide (ITO) or indium zinc oxide (IZO) as the recombination layer[12,16,18,45]. The disadvantage of the highly conductive recombination contact is that carriers will be more prone to being funnelled to any existent shunt pathways along the recombination layer[44], a problem that could limit scaling to larger areas. For this reason, a nanocrystalline hydrogenated Si (nc-Si:H) recombination layer using n+ and p+ doped layers has been deposited via low-temperature plasma-enhanced CVD compatible with silicon heterojunction (SHJ) solar cells[44], demonstrating higher shunt resistances and improved large-area performance in the resulting tandems. A similar approach resulted in the first 2T perovskite–Si tandem, where a narrow p++ / n++ junction on top of an n-type Si cell contacted the electron transporting TiO_2 layer in the perovskite solar cell[59]. A similar approach has yet to be demonstrated for the more commercially relevant p-type c-Si solar cells.

Compatible processing. In tandem solar cell processing, the first cell must remain intact during processing of the second cell, dictating the second subcell processing window. In the case of perovskite–Si tandems, the Si is always the substrate for the perovskite top cell. Most Si cells can withstand any temperature (up to 500 °C) and solvent that a perovskite deposition would require. The doped amorphous Si (a-Si) layer used to passivate the most efficient Si solar cells (SHJ), however, requires that the cell temperature remain below 200 °C. This makes it impossible to use the record (22.1%)[60] perovskite solar cell architecture comprising mesoporous TiO_2 layers, which require 500 °C sintering. As a result, the record 2T tandems on SHJ cells have been made by using only low-temperature processes for the perovskite cell deposition[18,41,42]. However, recently, an effective n-type homo-junction Si solar cell using SiN passivation layers and an interpenetrating metal/ITO recombination layer (Fig. 4c) allowed the most efficient top cells based on mesoporous TiO_2 to be used in tandems[45].

Processing a perovskite solar cell on top of another perovskite solar cell is difficult because the layers are more sensitive to temperature and solvents. To enable solution-processed perovskite layers, it is essential to use a protective layer between the two cells and to use only low-temperature processes. The protective layer should be conductive and serve as the recombination contact. We and others have used a sputtered ITO layer, which enabled the proof-of-principle demonstration of a 17% 2T perovskite tandem and, more recently, an 18.5% 2T perovskite tandem[12,16]. A completely solution processed 2T tandem[57] (including solution processed recombination layer)

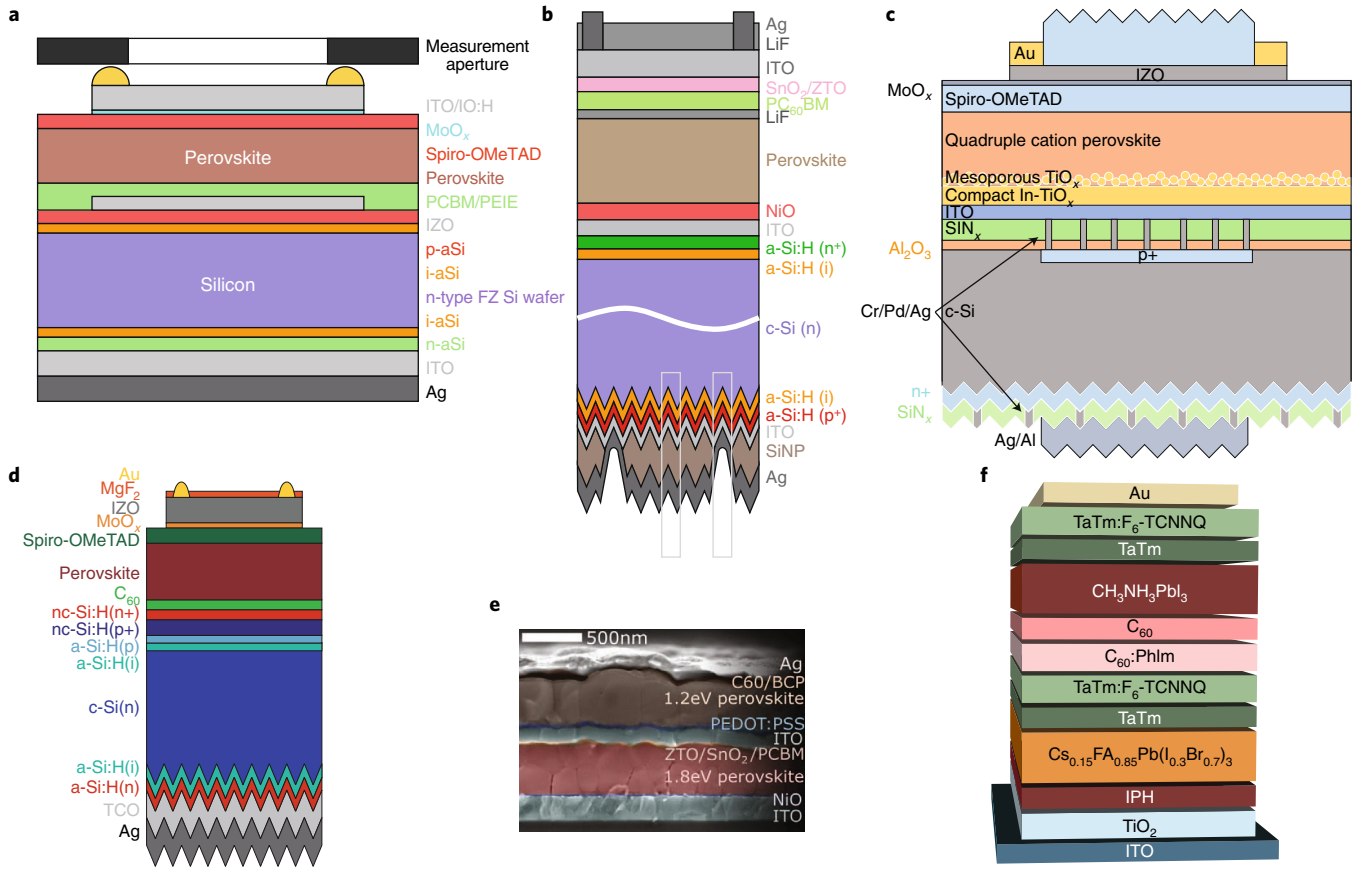

Fig. 4 | State-of-the-art tandem architectures. a–f, Selected monolithic tandem architectures (**a**–**d**, perovskite–Silicon; **e**,**f**, all-perovskite) are presented. Panels **a** and **b** show structures using SHJ Si cells, which limit the processing temperature to below 150 °C. The structure in panel **a** uses a MoO_x sputter buffer layer[41] for nip structure perovskite top cells, while panel **b** is in the pin structure and uses an SnO_2 sputter buffer layer[18]. Panel **c** uses an n-type homo-junction Si cell with SiN passivation and an interpenetrating metal/ITO recombination layer to enable high-temperature processing of the perovskite top cell[45]. Panel **d** uses a recombination layer made of n- and p-type nc-Si (ref. [44]). Panel **e** depicts a solution processed all-perovskite tandem with ITO recombination and protection layer[12], while panel **f** is a completely vapour-deposited all-perovskite tandem solar cell with an organic recombination layer[58]. Panels **a**–**f** adapted with permission from: ref. [41], American Chemical Society (**a**); ref. [18], Macmillan Publishers Ltd (**b**); ref. [45], RSC (**c**); ref. [44], Wiley (**d**); ref. [12], AAAS (**e**); ref. [58], Wiley (**f**).

would likely have to make use of cross-linked and doped organic layers, or uniform and impermeable metal oxide layers deposited by sol-gel processes. To date, such approaches have proven difficult. Making a fully dry, vapour-deposited tandem would provide a simpler path to a structure in which none of the layers damage one another. Thermal evaporation has recently been demonstrated[11,58] to be an effective route to depositing perovskites and recombination layers, but it has not yet been possible to evaporate perovskite layers with the ideal bandgap combination, limiting their tandem performance. The ability to co-evaporate the most promising bottom- and top-cell perovskites is complicated by the recent trend to use increasingly complex compositions using multiple A, B and X site species[12,60,61]. Developing vapour deposition routes for perovskites with ideal bandgaps is an exciting and scalable, though challenging, route to enable high-yield and efficient tandems.

Maximizing light harvesting. Effective light management is a key challenge in making efficient tandem solar cells. It is important to mitigate parasitic absorption by avoiding thick, absorbing contact layers such as doped Spiro-OMeTAD (hole transporter) and TCOs with much free-carrier absorption in the NIR[41,62–64]. While ITO is commonly used in perovskite tandems, higher mobility materials, such as IZO and H-InO_x (refs [63,65,66]), require lower doping concentrations to achieve the same sheet resistances and display lower parasitic absorption in a tandem. There is also significant parasitic absorption at interfaces with the reflective back contacts that can be recovered by ensuring they consist of materials with large differences in refractive index. For instance, it is possible to obtain an extra 1.5 mA cm^{-2} from the Si bottom cell by placing doped silicon nanoparticles between the a-Si and silver reflector layers[18].

Since perovskite solar cells comprise thin films, optical interference effects are very commonly observed in EQEs of perovskite tandem solar cells. This is especially true for the perovskite–perovskite tandems; several mA cm^{-2} are lost just due to optical interference effects[12,16]. Optical modelling[67,68] should enable rational design to minimize reflection peaks in the spectral response and even direct the IR part of the spectrum into the bottom cell and the visible into the top cell. Complex refractive indexes for most commonly used perovskite materials are available[29,30,67–69] and should guide such work. Materials with very low refractive indexes should be avoided in the middle of the tandem stack since these will result in large reflections at interfaces with the high-refractive index perovskite and Si subcells. The ITO recombination layer used in perovskite–Si tandems also induces reflectance losses to the Si subcell; for example, a nc-Si:H recombination layer has been shown to have significantly lower parasitic reflectance than an ITO recombination layer[44].

To fully remove reflection losses by improving light in-coupling and enhance the NIR response at the band edge, an ideal tandem

solar cell would also benefit from surface texturing. This is commonly realized in the form of several μm-sized pyramids etched into c-Si wafers. Such texture improves light in-coupling by minimizing reflections off the front surface while also scattering the light within the solar cell to enhance light trapping (enhancing path length and preventing escape through the front surface) and reduce optical interference to improve overall light harvesting. This can be easily done to the back surface of a c-Si bottom cell, but there exist no published examples of perovskite–Si tandems using c-Si bottom cells with both sides textured, despite the fact that commercial c-Si wafers are textured on top and bottom for maximum light trapping. Solution processing of perovskites does not enable conformal deposition over sharp features with several μm size. This limits the obtainable photocurrent in perovskite–silicon tandems by 1–2 mA cm^{-2} (ref. [70]). The most logical solution is to deposit the perovskite solar cell layers via a vapour deposition process that will conform to the sharp features of the texture. Alternatively, it is also possible to position an electrically inert but optically textured layer with appropriate refractive index directly on top of the top contact of the tandem solar cell to improve light harvesting[71].

Vapour processing would also enable perovskite–perovskite tandems to be deposited on pre-textured substrates. Such texturing may be the key to allowing perovskite–perovskite tandems to reach their full potential, both because of the low band-edge absorption in tin–lead perovskite absorber layers and because of the interference effects described above that will limit their light harvesting ability.

Scaling of perovskite tandem solar cells. Most of the tandem solar cells reported in the literature have been made at only 1 cm^2. This is in line with most of the perovskite solar cell research in general, and allows for the translation of spin-coating recipes optimized for single junctions to the tandem solar cells. Work at IMEC has demonstrated 4-cm^2 4-terminal tandem solar modules approaching 24%[72], but still used spin-coating for the perovskite subcell layers. There has been some progress on scaling single-junction perovskite modules by using various solution coating techniques, with a record of close to 16% measured through a 10 cm^2 aperture made through scalable blade coating[73]. With improved scribing, printed modules above 17% could be readily realized. This has been enabled by careful solvent engineering to widen the processing window, and the approach lends itself to low-cost manufacturing of the perovskite subcell. All-perovskite tandem solar cells could be printed in this way. However, the recombination layer would have to be impermeable and the module would be sensitive to any pinholes within the recombination layer. For this reason, obtaining high yields for solution-processed tandems may be a challenge. In addition, for reasons discussed above, commercial c-Si wafers are textured, which would prevent the use of blade-coated top cells unless they were planarized by an additional step. Currently, lab-scale tandem devices have planarized top surfaces for ease of perovskite deposition, but it is unclear whether this can easily be translated to a manufacturing context, and the planarization will result in less light trapping and lower photocurrents than could be achieved with texturing.

Another approach for making uniform large-area metal halide perovskites is vapour deposition[74]. However, it has proven difficult to make efficient materials with mixed A and B site compositions via direct co-evaporation. This issue can be sidestepped by first thermally evaporating the inorganic precursors (PbI_2 and CsI) and then converting them to perovskite by exposure to FAI/FABr precursors in methanol to achieve the desired composition[44], leading to the first large-area (12.96 cm^2) monolithic perovskite–silicon tandem solar cells. Efficient (15%) 12 cm^2 single-junction modules were recently reported[75] by vapour conversion of PbI_2 to $FAPbI_3$ and subsequent A site cation exchange (Cs replacing FA). Combining such a vapour conversion process with a thermally evaporated PbI_2/$PbBr_2$ layer could allow for a fully conformal and dry deposition technique. Such an approach would also be beneficial for all-perovskite tandems as none of the steps would damage underlying layers. Unfortunately, thermal evaporation at ultrahigh vacuum could be cost prohibitive, though a full cost analysis remains to be done. We suggest that research into rapid throughput vapour deposition of perovskite precursors should be a high priority for those attempting to scale tandem solar cells.

To make efficient large-area tandems, it is critical to use a recombination layer (such as nanocrystalline hydrogenated Si (nc-Si:H) n+ and p+ doped layers) with high sheet resistance to prevent leakage current funnelling through small shunt pathways[44]. For the same reason, less conductive recombination layers should be chosen for scaled all-perovskite tandems.

Reliability of tandem solar cells

While tandem solar cells offer opportunities for high PCEs, the requirements on perovskite bandgap and stack design also impose unique challenges for obtaining satisfactory stability. In addition, for perovskite–silicon tandems, use cases and stability requirements will be the same as those of high-efficiency crystalline Si solar cells today. All-perovskite tandem solar cells, with the opportunities for lightweight and flexible niche applications, may find uses that do not impose as stringent reliability requirements. This section highlights the technical challenges in improving the stability of perovskite tandem solar cells.

Perovskite–silicon tandems. For perovskites to be commercially viable and offer low levelized cost of electricity in tandems on silicon for rooftop and utility-scale installations, they must match silicon's 25-year lifetime. It is thus critical to examine whether tandem solar cells will require additional encapsulation over that used in conventional c-Si modules; if so, then this will have to be included in updated cost models to evaluate whether the added power output still validates the additional costs of making the tandem module.

While the X-site poses concerns of photoinstability[31] as discussed above, the A-site cation is often the focus of concerns regarding thermal, moisture and oxygen instability. The methylammonium cation is volatile but improved encapsulation has been shown to prevent its escape, enabling operation at elevated temperatures for hundreds of hours[43,47]. Formamidinium substitution shows improved thermal stability over methylammonium[13] and has also led to the highest-efficiency devices[27,28]. Further thermal stability improvement has been observed through either partial or full Cs substitution[76–81].

We have previously demonstrated that when such a stable perovskite composition is chosen, the organic A-site cation encapsulated by a conformal and dense TCO layer, and the full cell protected using industry standard processes using glass/glass packaging held together with butyl rubber edge seals and polymer encapsulants, perovskite cells can pass the International Electrotechnical Commission 'damp heat' test (1,000 h at 85% relative humidity at 85 °C)[18] and temperature cycling (−40 °C to 85 °C, 200 cycles)[82]. However, most commercial PV modules are subjected to three to five times these tests, so passing them once may not guarantee a 25 year lifetime for the full tandem. In addition, many c-Si modules currently use a Tedlar backsheet rather than glass on both the front and back; it remains to be seen whether the full tandem modules will require the use of two glass sheets, which could raise costs of the tandem module.

The ions in the perovskite top cell have been shown to be extremely mobile[83–85], while silicon surfaces are known to be very sensitive to contamination by impurities. It remains to be seen whether I^- can diffuse into the silicon subcell through the TCO recombination layer. This should be a subject for future studies, where the ion motion and potential light-induced compositional changes unique to perovskite solar cells may require the introduction of new stability standards.

All-perovskite tandems. A unique challenge for all-perovskite tandems is that they require some Sn^{2+} on the B-site of the small-bandgap bottom cell, but that Sn^{2+}, unlike Pb^{2+}, is susceptible to oxidation from the 2+ to the 4+ state on exposure to oxygen or moisture and has been reported to limit the lifetime of tin halide perovskites to be far shorter than that of their Pb counterparts[39,86,87]. However, we recently demonstrated that substitution of 50% or more (as is the case for compositions relevant to tandems) of the B site with an element other than tin (typically Pb) enhances the lifetime by a factor of 10–100 because it changes the oxidation mechanism of Sn to one less energetically favourable[40]. There have been no published studies of full device stability under heat or light in either ambient or inert conditions, so it is difficult to know whether the standard encapsulation used for Sn-free perovskites used in top cells and in perovskite–silicon tandems will suffice for the all-perovskite tandem. Certainly, if flexible form factors are desirable for all-perovskite tandems, flexible packaging will be a critical subject of research; currently available flexible packaging may be cost prohibitive.

All-perovskite tandems may also suffer from a unique instability: exchange of ions between the two perovskite layers. The A- and X-site cations especially have been shown to be mobile, so if the recombination layer does not provide a good ion diffusion barrier, it is possible that the Br ions will diffuse from the top cell to the bottom cell and that the composition of the subcells will homogenize over time, defeating the purpose of the tandem solar cell. This adds an extra constraint on the recombination layer choice. The TCO recombination layers currently used are very likely to provide protection, but it must be investigated whether this is enough for many years of operational stability or whether perfectly crack-free, dense, amorphous recombination layers must be developed.

An additional stability concern for tandem solar cells arises from the fact that they are composed of many layers, each of which could delaminate from the other. The adhesion between metal halide perovskites and the contact layers is extremely weak and the contact layers themselves (fullerenes in particular) suffer from weak internal adhesion[88]. This is especially worrying since the thermal expansion coefficients of the layers differs considerably[82]. Careful encapsulation with rigid glass/glass packages appears to mitigate this problem for single-junction devices and allows them to pass temperature cycling tests[82], but tandems contain even more layers. Tests will need to be performed on full tandem solar cells. Flexible all-perovskite tandem solar cells especially may be prone to delamination on bending and may require use of layers with stronger adhesion, perhaps through cross-linking strategies[89].

Outlook

Many of the pieces to enable efficient perovskite tandem solar cells at laboratory scale are in place. The present record open-circuit voltage of 1.24 V (for a perovskite single junction with 1.63 eV bandgap)[27] coupled with existing contacts and recombination layers should theoretically enable tandems in current architectures to attain PCEs of approximately 31% and 29.5% for perovskite–Si and perovskite–perovskite tandems, respectively.

As proof-of-concept laboratory-scale device records start to exceed those for perovskite single-junction solar cells, it will become important to consider the strategies used to reach those records holistically: can these same device structures and deposition processes be implemented on commercially relevant, stable tandems with high yield and low cost? This is an area of research where a simple translation of processes developed for single-junction modules may not deliver the desired results in tandem devices; coating on top of textured c-Si wafers remains an unsolved problem, while all-perovskite tandems may suffer from low yield when solution-coating is used for the perovskite layers.

Perhaps tandem-specific deposition routes should be explored; ideal routes would be high throughput, dry and conformally deposited, performed at ambient pressure or only mild vacuum, and easily adaptable to a wide range of perovskite compositions. The ease with which high-quality metal halide perovskite compounds are formed suggests that it should be possible to use alternative, high-throughput routes such as vapour transport deposition or closed space sublimation as used by the CdTe industry[90]. Though desirable, it is still unclear whether the metal halide components could be deposited via a high-throughput vapour phase deposition at atmospheric or mild pressures; this kind of deposition has not yet been attempted but may be an important area of research for those aiming to scale tandem solar cells. The organic A-site cations could be deposited through a spraying process, a blade-coating process or a vapour conversion process. In addition, tandem architectures currently require the use of thin buffer layers to prevent sputter damage during deposition of the TCOs, complicating device designs; the most efficient perovskite–silicon tandems currently employ seven steps, and more may be necessary if diffusion barriers prove to be essential to prevent metal ingress over long time scales. Again, the device designs need to be considered holistically to minimize the complexity, use scalable and cost effective deposition and materials, and ensure lifetimes compatible with 25 year operation.

Tandem module design has also gone largely unexplored by the academic community, despite the fact that tandem modules offer unique challenges. 2T architectures may be the simplest to implement from a module perspective, as they require fewer exterior electronics and will only require one cell size and form factor for the entire module. A 2T perovskite–Si module will look mostly exactly like that of a normal c-Si module, though attention may have to be given to how the cell interconnects are made: perovskite top cells may not be compatible with the soldering connections traditionally used in c-Si modules. A 2T perovskite–perovskite module could look identical to a single-junction perovskite module, consisting of monolithically interconnected cells in the form of long strips, but the exact design of the interconnects may have to be different to prevent shorting if a highly conductive recombination layer is used. 4T module designs are more complicated and allow for a greater range in designs. To enable either current or voltage matching between top and bottom modules, and reduce the reliance on exterior electronics, the size and number of series connected cells can be varied. Minimizing 'dead' area from shading by the top cell gridlines will also be an interesting engineering challenge.

Future work must focus on translating these proof-of-concept designs to scalable deposition processes, and on ensuring that industry standard packaging and encapsulation will suffice for tandem solar cells. Encapsulation of all-perovskite tandem solar cells especially requires significant research. Once this has been accomplished, perovskite–silicon tandems will be poised to be commercialized rapidly, benefiting from a partnership with the existing c-Si industry provided that the perovskite subcell does not limit the tandem stability. In the longer term, we believe all-perovskite tandems present the ultimate embodiment of perovskite technology, enabling highly-efficient and low-cost thin-film module manufacturing and deployment.

Received: 26 October 2017; Accepted: 22 May 2018;
Published online: 09 July 2018

References

1. Fu, R., Feldman, D. J., Margolis, R. M., Woodhouse, M. A. & Ardani, K. B. *US Solar Photovoltaic System Cost Benchmark: Q1 2017* (National Renewable Energy Laboratory, 2017).
2. Green, M. A. et al. Solar cell efficiency tables (version 50). *Prog. Photovolt. Res. Appl.* **25**, 668–676 (2017).
3. Frank, D. et al. Wafer bonded four-junction GaInP/GaAs//GaInAsP/GaInAs concentrator solar cells with 44.7% efficiency. *Prog. Photovolt. Res. Appl.* **22**, 277–282 (2014).

4. Chiu, P. T. et al. 35.8% space and 38.8% terrestrial 5J direct bonded cells. In *IEEE 40th Photovoltaic Specialist Conference* 11–13 (IEEE, 2014).
5. Contreras, M. A. et al. Wide bandgap Cu(In,Ga)Se2 solar cells with improved energy conversion efficiency. *Prog. Photovolt. Res. Appl.* **20**, 843–850 (2012).
6. Meillaud, F., Shah, A., Droz, C., Vallat-Sauvain, E. & Miazza, C. Efficiency limits for single-junction and tandem solar cells. *Sol. Energy Mater. Sol. Cells* **90**, 2952–2959 (2006).
7. Im, J.-H., Lee, C.-R., Lee, J.-W., Sang-Won, Park & Park, N.-G. 6.5% efficient perovskite quantum-dot-sensitized solar cell. *Nanoscale* **3**, 4088–4093 (2011).
8. Lee, M. M., Teuscher, J., Miyasaka, T., Murakami, T. N. & Snaith, H. J. Efficient hybrid solar cells based on meso-superstructured organometal halide perovskites. *Science* **338**, 643–647 (2012).
9. Kojima, A., Teshima, K., Shirai, Y. & Miyasaka, T. Organometal halide perovskites as visible-light sensitizers for photovoltaic cells. *J. Am. Chem. Soc.* **131**, 6050–6051 (2009).
10. Yang, M. et al. Perovskite ink with wide processing window for scalable high-efficiency solar cells. *Nat. Energy* **2**, 17038 (2017).
11. Momblona, C. et al. Efficient vacuum deposited pin and nip perovskite solar cells employing doped charge transport layers. *Energy Environ. Sci.* **9**, 3456–3463 (2016).
12. Eperon, G. E. et al. Perovskite-perovskite tandem photovoltaics with optimized bandgaps. *Science* **354**, 861–865 (2016).
This study presents a monolithic all-perovskite tandem solar cell with a low bandgap rear cell, 17% efficiency and promising stability.
13. Eperon, G. E. et al. Formamidinium lead trihalide: A broadly tunable perovskite for efficient planar heterojunction solar cells. *Energy Environ. Sci.* **7**, 982–988 (2014).
14. Hao, F., Stoumpos, C. C., Chang, R. P. H. & Kanatzidis, M. G. Anomalous band gap behavior in mixed Sn and Pb perovskites enables broadening of absorption spectrum in solar cells. *J. Am. Chem. Soc.* **136**, 8094–8099 (2014).
15. Unger, E. L. et al. Roadmap and roadblocks for the band gap tunability of metal halide perovskites. *J. Mater. Chem. A* **5**, 11401–11409 (2017).
16. Rajagopal, A. et al. Highly efficient perovskite–perovskite tandem solar cells reaching 80% of the theoretical limit in photovoltage. *Adv. Mater.* **29**, 1521–4095 (2017).
This work demonstrates monolithic all-perovskite tandem solar cells with high voltages approaching 2 V, nearing the thermodynamic limit and demonstrating the potential of all-perovskite tandem solar cells.
17. Zhao, D. et al. Low-bandgap mixed tin–lead iodide perovskite absorbers with long carrier lifetimes for all-perovskite tandem solar cells. *Nat. Energy* **2**, 17018 (2017).
18. Bush, K. A. et al. 23.6%-efficient monolithic perovskite/silicon tandem solar cells with improved stability. *Nat. Energy* **2**, 17009 (2017).
This study presents the current record perovskite–silicon 2T tandem, made with perovskite front cells that can pass IEC standard accelerated aging tests at 85% relative humidity at 85 °C for 1,000 hours.
19. Duong, T. et al. Rubidium multication perovskite with optimized bandgap for perovskite-silicon tandem with over 26% efficiency. *Adv. Energy Mater.* **7**, 1700228 (2017).
This work illustrates the use of a quadruple cation perovskite composition to make 26.4% 4T perovskite–silicon tandem solar cells, which is very close the single junction c-Si record efficiency of 26.6%.
20. Yoshikawa, K. et al. Silicon heterojunction solar cell with interdigitated back contacts for a photoconversion efficiency over 26%. *Nat. Energy* **2**, 17032 (2017).
21. *Best Research-Cell Efficiencies* (NREL, 2018); https://www.nrel.gov/pv/assets/images/efficiency-chart.png
22. Yu, Z., Leilaeioun, M. & Holman, Z. Selecting tandem partners for silicon solar cells. *Nat. Energy* **1**, 16137 (2016).
23. Taguchi, M. et al. 24.7% record efficiency HIT solar cell on thin silicon wafer. *IEEE J. Photovolt.* **4**, 96–99 (2014).
24. Rajagopal, A., Liang, P.-W., Chueh, C.-C., Yang, Z. & Jen, A. K.-Y. Defect passivation via graded fullerene heterojunction in low bandgap Pb-Sn binary perovskite photovoltaics. *ACS Energy Lett.* **2**, 2531–2539 (2017).
25. Noel, N. K. et al. Unveiling the influence of pH on the crystallization of hybrid perovskites, delivering low voltage loss photovoltaics. *Joule* **1**, 328–343 (2017).
26. Wang, Z. et al. Efficient ambient-air-stable solar cells with 2D–3D heterostructured butylammonium-caesium-formamidinium lead halide perovskites. *Nat. Energy* **2**, 17135 (2017).
27. Saliba, M. et al. Incorporation of rubidium cations into perovskite solar cells improves photovoltaic performance. *Science* **354**, 206–209 (2016).
In this paper, the authors present a wide bandgap (1.63 eV) perovskite composition with the highest voltage output of any existing efficient perovskite solar cell, making it suitable as a top cell for tandem applications.
28. Yang, W. S., Park, B., Jung, E. H. & Jeon, N. J. Iodide management in formamidinium-lead-halide-based perovskite layers for efficient solar cells. **1379**, 1376–1379 (2017).
29. Maximilian Hoerantner, H. J. S. Predicting and optimising the energy yield of perovskite-on-silicon tandem solar cells under real world conditions. *Energy Environ. Sci.* **10**, 1983–1993 (2017).
30. Hörantner, M. T. et al. The potential of multijunction perovskite solar cells. *ACS Energy Lett.* **2**, 2506–2513 (2017).
31. Hoke, E. T. et al. Reversible photo-induced trap formation in mixed-halide hybrid perovskites for photovoltaics. *Chem. Sci.* **6**, 613–617 (2015).
32. Slotcavage, D. J., Karunadasa, H. I. & McGehee, M. D. Light-induced phase segregation in halide-perovskite absorbers. *ACS Energy Lett.* **1**, 1199–1205 (2016).
33. Abdi-Jalebi, M. et al. Maximizing and stabilizing luminescence from halide perovskites with potassium passivation. *Nature* **555**, 497 (2018).
34. Yang, Z. et al. Stable low-bandgap PbSn binary perovskites for tandem solar cells. *Adv. Mater.* **28**, 8990–8997 (2016).
35. Liao, W. et al. Fabrication of efficient low-bandgap perovskite solar cells by combining formamidinium tin iodide with methylammonium lead iodide. *J. Am. Chem. Soc.* **138**, 12360–12363 (2016).
36. Ogomi, Y. et al. $CH_3NH_3SnxPb(1-x)I_3$ perovskite solar cells covering up to 1060 nm. *J. Phys. Chem. Lett.* **5**, 1004–1011 (2014).
37. Prasanna, R. et al. Band gap tuning via lattice contraction and octahedral tilting in perovskite materials for photovoltaics. *J. Am. Chem. Soc.* **139**, 11117–11124 (2017).
38. Zhao, B. et al. High open-circuit voltages in tin-rich low-bandgap perovskite-based planar heterojunction photovoltaics. *Adv. Mater.* **29**, 1604744 (2016).
39. Noel, N. K. et al. Lead-free organic-inorganic tin halide perovskites for photovoltaic applications. *Energy Environ. Sci.* **7**, 3061–3068 (2014).
40. Leijtens, T., Prasanna, R., Gold-Parker, A., Toney, M. F. & McGehee, M. D. Mechanism of tin oxidation and stabilization by lead substitution in tin halide perovskites. *ACS Energy Lett.* **9**, 2159–2165 (2017).
41. Werner, J. et al. Efficient monolithic perovskite/silicon tandem solar cell with cell area >1 cm^2. *J. Phys. Chem. Lett.* **7**, 161–166 (2016).
42. Albrecht, S. et al. Monolithic perovskite/silicon-heterojunction tandem solar cells processed at low temperature. *Energy Environ. Sci.* **9**, 81–88 (2016).
43. Bush, K. A. et al. Thermal and environmental stability of semi-transparent perovskite solar cells for tandems enabled by a solution-processed nanoparticle buffer layer and sputtered ITO electrode. *Adv. Mater.* (2016).
44. Sahli, F. et al. Improved optics in monolithic perovskite/silicon tandem solar cells with a nanocrystalline silicon recombination junction. *Adv. Energy Mater.* **8**, 1701609 (2018).
45. Wu, Y. et al. Monolithic perovskite/silicon-homojunction tandem solar cell with over 22% efficiency. *Energy Environ. Sci.* **10**, 2472–2479 (2017).
46. Leijtens, T. et al. Stability of metal halide perovskite solar cells. *Adv. Energy Mater.* **5**, 1500963 (2015).
47. Brinkmann, K. O. et al. Suppressed decomposition of organometal halide perovskites by impermeable electron-extraction layers in inverted solar cells. *Nat. Commun.* **8**, 13938 (2017).
48. Leijtens, T. et al. Towards enabling stable lead halide perovskite solar cells; interplay between structural, environmental, and thermal stability. *J. Mater. Chem. A* **5**, 11483–11500 (2017).
49. Azpiroz, J. M., Mosconi, E., Bisquert, J. & De Angelis, F. Defect migration in methylammonium lead iodide and its role in perovskite solar cell operation. *Energy Environ. Sci.* **8**, 2118–2127 (2015).
50. Domanski, K. et al. Not all that glitters is gold: Metal-migration-induced degradation in perovskite solar cells. *ACS Nano* **10**, 6306–6314 (2016).
51. Kim, I. S. & Martinson, A. B. F. Stabilizing hybrid perovskites against moisture and temperature via non-hydrolytic atomic layer deposited overlayers. *J. Mater. Chem. A* **3**, 20092–20096 (2015).
52. Conings, B. et al. Intrinsic thermal instability of methylammonium lead trihalide perovskite. *Adv. Energy Mater.* **5**, 1500477 (2015).
53. Bella, F. et al. Improving efficiency and stability of perovskite solar cells with photocurable fluoropolymers. *Science* **354**, 203–206 (2016).
54. Cotal, H. et al. III-V multijunction solar cells for concentrating photovoltaics. *Energy Environ. Sci.* **2**, 174–192 (2009).
55. Takamoto, T., Ikeda, E., Kurita, H. & Ohmori, M. Over 30% efficient InGaP/GaAs tandem solar cells. *Appl. Phys. Lett.* **70**, 381–383 (1997).
56. Chang, C. Y. et al. Highly efficient polymer tandem cells and semitransparent cells for solar energy. *Adv. Energy Mater.* **4**, 1–6 (2014).
57. Jiang, F. et al. A two-terminal perovskite/perovskite tandem solar cell. *J. Mater. Chem. A* **4**, 1208–1213 (2016).
58. Forgács, D. et al. Efficient monolithic perovskite/perovskite tandem solar cells. *Adv. Energy Mater.* **7**, 1602121 (2017).
59. Mailoa, J. P. et al. A 2-terminal perovskite / silicon multijunction solar cell enabled by a silicon tunnel junction. *Appl. Phys. Lett.* **106**, 121105 (2015).
60. Yang, W. S. et al. Iodide management in formamidinium-lead-halide–based perovskite layers for efficient solar cells. *Science* **356**, 1376–1379 (2017).

61. Saliba, M. et al. Cesium-containing triple cation perovskite solar cells: improved stability, reproducibility and high efficiency. *Energy Environ. Sci.* **9**, 1989–1997 (2016).
62. Margulis, G. Y., Hardin, B. E., Ding, I. K., Hoke, E. T. & McGehee, M. D. Parasitic absorption and internal quantum efficiency measurements of solid-state dye sensitized solar cells. *Adv. Energy Mater.* **3**, 959–966 (2013).
63. Phillips, J. M. et al. Zinc-indium-oxide: a high conductivity transparent conducting oxide. *Appl. Phys. Lett.* **67**, 2246–2248 (1995).
64. Rech, S. A. et al. Towards optical optimization of planar monolithic perovskite/silicon-heterojunction tandem solar cells. *J. Opt.* **18**, 64012 (2016).
65. Gordon, R. G. Criteria for choosing transparent conductors. *MRS Bull.* **25**, 52–57 (2000).
66. Leenheer, A. J. et al. General mobility and carrier concentration relationship in transparent amorphous indium zinc oxide films. *Phys. Rev. B* **77**, 115215 (2008).
67. Löper, P. et al. Complex refractive index spectra of $CH_3NH_3PbI_3$ perovskite thin films determined by spectroscopic ellipsometry and spectrophotometry. *J. Phys. Chem. Lett.* **6**, 66–71 (2015).
68. Lin, Q., Armin, A., Nagiri, R. C. R., Burn, P. L. & Meredith, P. Electro-optics of perovskite solar cells. *Nat. Photon.* **9**, 106–112 (2015).
69. Ball, J. M. M. et al. Optical properties and limiting photocurrent of thin-film perovskite solar cells. *Energy Environ. Sci.* **8**, 602–609 (2015).
70. Santbergen, R. et al. Minimizing optical losses in monolithic perovskite/c-Si tandem solar cells with a flat top cell. *Opt. Express* **24**, A1288–A1299 (2016).
71. Manzoor, S. et al. Solar energy materials and solar cells improved light management in planar silicon and perovskite solar cells using PDMS scattering layer. *Sol. Energy Mater. Sol. Cells* **173**, 59–65 (2017).
72. Imec reports record conversion efficiency of 23.9 percent on a 4cm² perovskite/silicon solar module. *Imec* https://go.nature.com/2H5hNiK (2017).
73. Yang, M. et al. Highly efficient perovskite solar modules by scalable fabrication and interconnection optimization. *ACS Energy Lett.* **3**, 322–328 (2018).
74. Borchert, J. et al. Large-area, highly uniform evaporated formamidinium lead triiodide thin films for solar cells. *ACS Energy Lett.* **2**, 2799–2804 (2017).
75. Jiang, Y. et al. Combination of hybrid CVD and cation exchange for upscaling Cs-substituted mixed cation perovskite solar cells with high efficiency and stability. *Adv. Funct. Mater.* **28**, 1703835 (2018).
76. Li, Z. et al. Stabilizing perovskite structures by tuning tolerance factor: Formation of formamidinium and cesium lead iodide solid-state alloys. *Chem. Mater.* **28**, 284–292 (2016).
77. Lee, J.-W. et al. Formamidinium and Cesium hybridization for photo- and moisture-stable perovskite solar cell. *Adv. Energy Mater.* **5**, 1501310 (2015).
78. Sutton, R. J. et al. Bandgap-tunable cesium lead halide perovskites with high thermal stability for efficient solar cells. *Adv. Energy Mater.* **6**, 1502458 (2016).
79. Choi, H. et al. Cesium-doped methylammonium lead iodide perovskite light absorber for hybrid solar cells. *Nano Energy* **7**, 80–85 (2014).
80. Beal, R. E. et al. Cesium lead halide perovskites with improved stability for tandem solar cells. *J. Phys. Chem. Lett.* **7**, 746–751 (2016).
81. McMeekin, D. P. et al. A mixed-cation lead mixed-halide perovskite absorber for tandem solar cells. *Science* **351**, 151–155 (2016).
This study demonstrates a range of efficient wide bandgap perovskite composition by alloying formamidinium and cesium on the A site.
82. Cheacharoen, R. et al. Design and understanding of encapsulated perovskite solar cells to withstand temperature cycling. *Energy Environ. Sci.* **11**, 144–150 (2018).
83. deQuilettes, D. W. et al. Photo-induced halide redistribution in organic–inorganic perovskite films. *Nat. Commun.* **7**, 11683 (2016).
84. Leijtens, T. et al. Mapping electric field – induced switchable polarization and structural degradation in hybrid lead halide perovskite thin films. *Adv. Energy Mater.* **5**, 1500962 (2015).
85. Yun, J. S. et al. Critical role of grain boundaries for ion migration in formamidinium and methylammonium lead halide perovskite solar cells. *Adv. Energy Mater.* **6**, 1600330 (2016).
86. Takahashi, Y. et al. Charge-transport in tin-iodide perovskite $CH_3NH_3SnI_3$: origin of high conductivity. *Dalton Trans.* **40**, 5563–5568 (2011).
87. Hao, F., Stoumpos, C. C., Cao, D. H., Chang, R. P. H. & Kanatzidis, M. G. Lead-free solid-state organic-inorganic halide perovskite solar cells. *Nat. Photon.* **8**, 489–494 (2014).
88. Rolston, N. et al. Mechanical integrity of solution-processed perovskite solar cells. *Extrem. Mech. Lett.* **9**, 353–358 (2016).
89. Watson, B. L. et al. Cross-linkable, solvent-resistant fullerene contacts for robust and efficient perovskite solar cells with increased JSC and VOC. *ACS Appl. Mater. Interfaces* **8**, 25896–25904 (2016).
90. Anthony, T. C., Fahrenbruch, A. L. & Bube, R. H. Growth of CdTe films by close-spaced vapor transport. *J. Vac. Sci. Technol. A Vac., Surf. Film.* **2**, 1296–1302 (1984).
91. Werner, J. et al. Efficient near-infrared-transparent perovskite solar cells enabling direct comparison of 4-terminal and monolithic perovskite/silicon tandem cells. *ACS Energy Lett.* **1**, 474–480 (2016).
92. Bailie, C. D. et al. Semi-transparent perovskite solar cells for tandems with silicon and CIGS. *Energy Environ. Sci.* **8**, 956–963 (2015).
93. Zhao, D. et al. Four-terminal all-perovskite tandem solar cells achieving power conversion efficiencies exceeding 23%. *ACS Energy Lett.* **3**, 305–306 (2018).
This study gives a demonstration of an all-perovskite tandem solar cell (4T) exceeding the performance record of the best single-junction perovskite solar cell.
94. Song, Z. et al. A technoeconomic analysis of perovskite solar module manufacturing with low-cost materials and techniques. *Energy Environ. Sci.* **10**, 1297–1305 (2017).
95. Chang, N. L. et al. A manufacturing cost estimation method with uncertainty analysis and its application to perovskite on glass photovoltaic modules. *Prog. Photovolt. Res. Appl.* **25**, 390–405 (2017).
96. Cai, M. et al. Cost-performance analysis of perovskite solar modules. *Adv. Sci.* **4**, 1600269 (2017).
97. Horowitz, K. A. W., Fu, R. & Woodhouse, M. An analysis of glass–glass CIGS manufacturing costs. *Sol. Energy Mater. Sol. Cells* **154**, 1–10 (2016).
98. Horowitz, K. A. W. & Woodhouse, M. Cost and potential of monolithic CIGS photovoltaic modules. In *IEEE 42nd Photovoltaic Specialist Conference* 1–6 (IEEE, 2015).
99. Woodhouse, M. et al. Perspectives on the pathways for cadmium telluride photovoltaic module manufacturers to address expected increases in the price for tellurium. *Sol. Energy Mater. Sol. Cells* **115**, 199–212 (2013).
100. Werner, J., Niesen, B. & Ballif, C. Perovskite/silicon tandem solar cells: Marriage of convenience or true love story? – An overview. *Adv. Mater. Interfaces* **5**, 1700731 (2017).
101. Duck, B. C. et al. Energy yield potential of perovskite-silicon tandem devices. In *IEEE 43rd Photovoltaic Specialists Conference* 1624–1629 (IEEE, 2016).
102. Shockley, W. & Queisser, H. J. Detailed balance limit of efficiency of p-n junction solar cells. *J. Appl. Phys.* **32**, 510 (1961).
103. Sheng, R. et al. Methylammonium lead bromide perovskite-based solar cells by vapor-assisted deposition. *J. Phys. Chem. C.* **119**, 3545–3549 (2015).
104. Nam, J. K. et al. Potassium incorporation for enhanced performance and stability of fully inorganic cesium lead halide perovskite solar cells. *Nano Lett.* **17**, 2028–2033 (2017).

Acknowledgements

We thank Department of Energy (DOE) SunShot and Office of Naval Research (ONR) for funding. T.L. is supported by a Marie Curie fellowship under Horizon 2020, and K.A.B. is supported by a National Science Foundation (NSF) fellowship.

Competing interests

The authors declare no competing interests.

Additional information

Supplementary information is available for this paper at https://doi.org/10.1038/s41560-018-0190-4.

Reprints and permissions information is available at www.nature.com/reprints.

Correspondence should be addressed to T.L. or M.D.M.

Publisher's note: Springer Nature remains neutral with regard to jurisdictional claims in published maps and institutional affiliations.